

## Chapter 3

# NURBS-based Discrete Element Method

The two major components of the proposed NURBS-based DEM are the use of NURBS for representing particle geometries, and the contact algorithm for determining the signed gap or penetration between two non-convex NURBS surfaces. We discuss these two components in detail in this chapter.

### 3.1 Non-Uniform Rational Basis-Splines (NURBS)

Non-Uniform Rational Basis-Splines (NURBS) are ubiquitous in the world of computer graphics, computer-aided design (CAD), computer-aided engineering (CAE), and computer-aided manufacturing (CAM) systems, as well as in computer animations. These functions provide great flexibility in representing arbitrary and complex geometries with much less information than conventional faceted or polynomial counterparts. Perhaps more importantly, in the context of this work and as shown in this section, the mathematical properties of NURBS make them ideal candidates for the description of grain morphology, the integration of discrete equations of motion, and the detection of contact.

In what follows we briefly describe the essential components of NURBS in the context of the current application. The literature on NURBS is extensive and relatively mature, and our purpose here is not to present all of its elements but rather those that are needed for completeness of presentation. For an exhaustive description of NURBS the reader is referred to [48; 84–86], whose presentation and notational convention we follow closely. We adhere to the convention in the computational geometry literature where the degree

$p = 1, 2, 3$ , etc. refers to constant, linear, quadratic, cubic, etc., piecewise polynomials, respectively. In the following incomplete description of NURBS, we split the acronym into three parts: Non-Uniform (NU), Rational (R), and Basis-Splines (BS). We describe these parts in reverse order and incrementally for clarity of presentation.

### 3.1.1 Basis-Splines (BS)

Within the description of Basis-Splines (B-Splines), there are three main elements necessitated [86]:

1. A set of  $n + 1$  control points  $\mathbf{P}_i$  ( $0 \leq i \leq n$ ),
2. A knot vector  $U$  of  $m + 1$  knots ( $0 = u_0 \leq u_1 \leq \dots \leq u_{m-1} \leq u_m = 1$ ), and
3. A degree  $p$  satisfying  $m = n + o$  where  $o = p + 1$  is the order of the curve.

Note that the last requirement means that the number of knots  $m + 1$  must be equal to the number of control points  $n + 1$  plus the curve order  $p + 1$ . The control points need not lie on the curve itself. Rather, control points act as a scaffold that controls the geometry [48]. At the most rudimentary level, one manipulates the geometry by adjusting the control points until the desired shape is met. Piecewise linear interpolation of the control points effectively furnishes a control polygon bounding the geometry.

Given the aforementioned parameters, a (non-rational, polynomial) B-Spline curve is defined parametrically as

$$\mathbf{C}(u) = \sum_{i=0}^n N_{i,p}(u) \mathbf{P}_i \quad (3.1)$$

where  $u$  is the curve parameter, and  $N_{i,p}$  is the  $i$ -th B-Spline basis function of degree  $p$  defined recursively as follows:

$$\begin{aligned} N_{i,0}(u) &= \begin{cases} 1 & \text{if } u \in [u_i, u_{i+1}) \\ 0 & \text{otherwise} \end{cases} \\ N_{i,p}(u) &= \frac{u - u_i}{u_{i+p} - u_i} N_{i,p-1}(u) + \frac{u_{i+p+1} - u}{u_{i+p+1} - u_{i+p}} N_{i+1,p-1}(u) \end{aligned} \quad (3.2)$$

The above is also known as the Cox-de Boor recursion formula [87; 88].

### 3.1.2 Rational B-Splines (RBS)

A known limitation of (non-rational) B-Splines, as defined in equation (3.1), is their inability to capture conic sections (e.g., circles and ellipses). This limitation stems from the simple polynomial form of B-Splines. To be able to represent conic sections, the parametric form would need to be *rational*, i.e., the quotient of two polynomials. A rational B-Spline (RBS) is furnished by adding a weight  $w_i \geq 0$ , which provides an additional degree of freedom for geometry manipulation. Hence, the curve equation becomes

$$\mathbf{C}(u) = \frac{\sum_{i=0}^n N_{i,p}(u)w_i \mathbf{P}_i}{\sum_{i=0}^n N_{i,p}(u)w_i} \quad (3.3)$$

$$= \sum_{i=0}^n R_{i,p}(u) \mathbf{P}_i \quad (3.4)$$

where  $R_{i,p}(u) = N_{i,p}(u)w_i / (\sum_{i=0}^n N_{i,p}(u)w_i)$ ,  $0 \leq i \leq n$ , are the rational basis functions. Since  $R_{i,p}(u)$  is rational, the exact description of conic sections becomes possible. Naturally, when all weights are equal to unity, equation (3.4) reduces to equation (3.1).

It is interesting to note the geometric contribution of the weights. The weight  $w_k$  affects the effective contribution of control point  $\mathbf{P}_k$  on the overall shape of the curve  $\mathbf{C}(u)$ . Making  $w_k$  smaller corresponds to ‘pushing’ the curve away from the control point  $\mathbf{P}_k$ . In the extreme, when  $w_k = 0$ , the term  $w_k \mathbf{P}_k$  is annihilated from the equation of the curve and the contribution of the control point is obviously nullified. Another interesting extreme is obtained by making  $w_k$  very large relative to other weights. Dividing equation (3.4) by  $w_k$  gives

$$\mathbf{C}(u) = \frac{\sum_{i \neq k}^n N_{i,p}(u)w_i/w_k \mathbf{P}_i + N_{k,p}(u)\mathbf{P}_k}{\sum_{i \neq k}^n N_{i,p}(u)w_i/w_k + N_{k,p}(u)} \quad (3.5)$$

where one can see that as  $w_k$  is increased, the curve  $\mathbf{C}(u)$  is ‘pulled’ towards the control point  $\mathbf{P}_k$ .

**Remark 3.1.1** *In the context of grain modeling, the inability of non-rational B-Splines to represent conic sections should not be viewed as a disadvantage, since real grains are rarely spherical or circular in section. NURBS can be used in their simpler polynomial B-spline version when their full power is not necessary.*

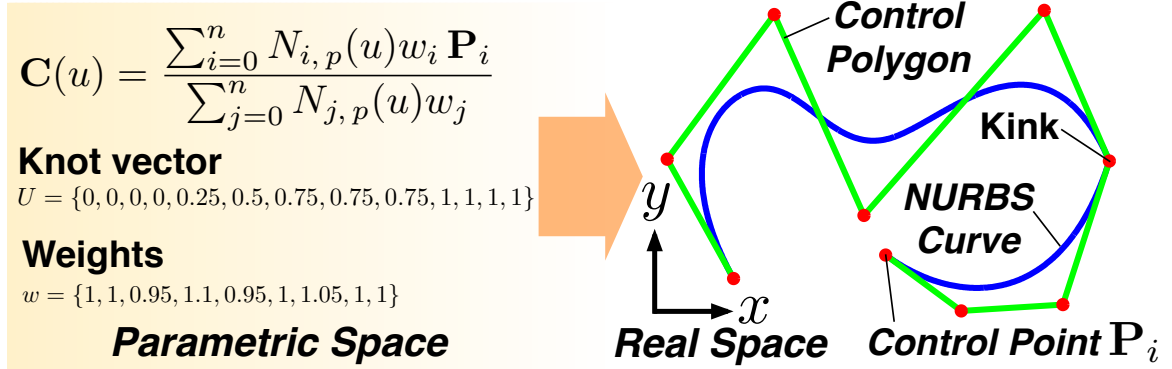


Figure 3.1: Schematic illustration of a NURBS curve. The curve degree  $p$  is 3 (cubic). The knots  $u_i$  and weights  $w_j$  are listed in the vectors  $U$  and  $w$ , respectively. The kink in the curve is due to full multiplicity  $k = p = 3$ , in which the knot/parameter value  $u = 0.75$  is repeated  $p = 3$  times.

### 3.1.3 Non-Uniform (NU) Rational B-Splines (NURBS)

The NU portion in NURBS is furnished by the knots in the knot vector  $U$  of the B-Splines. The non-decreasing knots  $u_i$ ,  $i = 0, 1, \dots, m$  partitions the parameter space into segments of half-open intervals  $[u_i, u_{i+1})$ , which are also called knot spans. The knot span can be of zero length since the knots need not be distinct, i.e., they can be repeated. The number of times a knot value repeats itself is called multiplicity  $k$ . Based on the way the knots are spaced, we can divide B-Splines into the following types:

1. Uniform B-Splines, which can be subdivided into non-periodic and periodic
2. Non-uniform B-Splines

In non-periodic uniform B-Splines, the knots are uniformly spaced except at the ends where the knot values are repeated  $p + 1$  times, so that

$$U = \{\underbrace{0, 0, \dots, 0}_{p+1}, u_{p+1}, \dots, u_{m-p-1}, \underbrace{\alpha, \alpha, \dots, \alpha}_{p+1}\} \quad (3.6)$$

The above knots are also referred to as non-periodic or open knots. Non-periodic B-Splines are infinitely continuously differentiable in the interior of a knot span, and  $(p - k)$ -times continuously differentiable at a knot. If  $k = p$ , we say that the knot has full multiplicity; the multiplicity cannot be greater than the degree. Multiplicity of knots provides a way to specify the continuity order between segments. For example, a full multiplicity knot in the

knot vector (away from the ends) means that a kink or cusp is present in the curve. On the other hand, in periodic B-Splines, the knots are uniformly spaced but the first and last knots are not duplicated, so that the knot vector looks like

$$U = \{0, 1, \dots, n\} \quad (3.7)$$

Periodic B-Splines are everywhere  $(p - 1)$ -times continuously differentiable.

If the knots are unequally spaced, the knot vector is non-uniform, we get non-uniform B-Splines (the NU part in NURBS). The non-uniformity in knots can cause the degree  $p$  of the curve to be different between knot spans. As a matter of terminology and in describing grain geometries, knot vectors can be defined in either  $[0, 1]$  or  $[0, n]$ . The choice of normalization does not have any effect on the shape of the curve, and it is therefore inconsequential. A schematic of a NURBS curve is shown in Figure 3.1.

**Remark 3.1.2** *Equation (3.3) is usually taken as the definition of NURBS, although the non-uniformity of the knots is not obvious from this expression.*

**Remark 3.1.3** *Several NURBS CAD technologies, such as Rhino [89], which are already available for geometric design of engineering components could be directly integrated into the modeling pipeline, facilitating the transition from binary data to models of granular assemblies.*

**Remark 3.1.4** *It is rare that one would work with NURBS models directly in parametric space. In practice, grain shapes are typically generated interactively or through some optimization procedure such as least squares.*

### 3.1.4 Closing a NURBS curve

To reproduce grain geometries accurately, it is necessary to close the NURBS curves used to describe the grain boundary. There are at least two procedures to close a NURBS curve. In the first procedure, closed NURBS curves are defined by ‘wrapping’ control points. In this process, a uniform knot sequence of  $m + 1$  knots is constructed such that:  $u_0 = 0, u_1 = 1/m, u_2 = 2/m, \dots, u_m = 1$ . Note that the domain of the curve is  $[u_p, u_{n-p}]$ . Then, the first and last  $p$  control points are wrapped so that  $\mathbf{P}_0 = \mathbf{P}_{n-p+1} = \mathbf{P}_{n-p+2}, \dots, \mathbf{P}_{p-2} = \mathbf{P}_{n-1}$

and  $\mathbf{P}_{p-1} = \mathbf{P}_n$ . By wrapping the control points,  $C^{p-1}$  continuity is ensured at the joining point  $\mathbf{C}(u_p) = \mathbf{C}(u_{n-p})$ .

In the second approach, the first and last control points are made coincident, i.e.,  $\mathbf{P}_0 = \mathbf{P}_n$  and the first and last  $p+1$  knots are clamped, i.e., repeated. The curve may or may not have  $C^k$  continuity depending on how the first and last  $k$  internal knot spans are chosen, and the first and last  $k+1$  weights and control points are chosen. Perhaps the simplest example is that of a unit circle in which the control points and weights shown in Table 3.1 are used together with the following knot vector:

$$U = \{0, 0, 0, 1, 1, 2, 2, 3, 3, 4, 4, 4\} \quad (3.8)$$

We notice that  $\mathbf{P}_0 = \mathbf{P}_8$  and the first and last three knot values are clamped. Also, there are three pairs of internal knots with multiplicity two. In general, this would lead to a loss of continuity in the first derivative. However, in this case, continuity in the first derivative is maintained by three collinear control points in each of the following sets:  $\{\mathbf{P}_7, \mathbf{P}_0 = \mathbf{P}_8, \mathbf{P}_1\}$ ,  $\{\mathbf{P}_1, \mathbf{P}_2, \mathbf{P}_3\}$ ,  $\{\mathbf{P}_3, \mathbf{P}_4, \mathbf{P}_5\}$ , and  $\{\mathbf{P}_5, \mathbf{P}_6, \mathbf{P}_7\}$ . In this work, we will use knot vectors that are clamped.

$i$	$x_i$	$y_i$	$w_i$
0	1	0	1
1	1	1	$\sqrt{2}/2$
2	0	1	1
3	-1	1	$\sqrt{2}/2$
4	-1	0	1
5	-1	-1	$\sqrt{2}/2$
6	0	-1	1
7	1	-1	$\sqrt{2}/2$
8	1	0	1

Table 3.1: Control points  $(x_i, y_i)$  and weights  $w_i$  for a unit circle.

### 3.1.5 NURBS surfaces

In 3D, we describe the grain geometry as a tensor product surface, with the coordinates of the NURBS surface in real space given by components of the vector:

$$\mathbf{Y}(u, v) = \sum_{i=0}^m \sum_{j=0}^n \left( \frac{w_{ij} N_{i,p}(u) N_{j,p}(v)}{\sum_{g=0}^m \sum_{h=0}^n w_{gh} N_{g,p}(u) N_{h,p}(v)} \right) \mathbf{P}_{ij} \quad (3.9)$$

where  $\mathbf{P}_{ij}$  are the control points,  $w_{ij}$  are the weights, and  $N_{i,p}(u)$  and  $N_{j,p}(v)$  are the B-Splines univariate basis functions of degree  $p$ . We must therefore specify a knot vector for the  $u$  basis functions, and a second knot vector for the  $v$  basis functions. Although there is no restriction on the choice of degree, we have restricted to NURBS surfaces of (cubic) degree  $p = 3$  in our applications.

### 3.1.6 Relevance of NURBS to DEM calculations

To conclude this section, some of the advantages of using NURBS in the context of DEM calculations are listed. Some of the most salient mathematical properties of NURBS that make them ideal candidates for DEM calculations are [48; 84]:

1. Local support property
2. Invariance under affine transformations
3. Strong convex hull property
4. Local curvature equation
5. Integration with isogeometric analysis

The local support property affords the method tremendous flexibility in the description of grain geometries. For example, in the case of NURBS curves, local support implies that the basis function  $N_{i,p}(u)$  is non-zero on  $[u_i, u_{i+p+1})$ . Since the basis function  $N_{i,p}(u)$  is the coefficient of control point  $\mathbf{P}_i$ , the product  $N_{i,p}(u)\mathbf{P}_i$  changes if  $\mathbf{P}_i$  changes, but the change in  $N_{i,p}(u)\mathbf{P}_i$  only affects the segment on  $[u_i, u_{i+p+1})$ , leaving the rest of the curve  $\mathbf{C}(u)$  unchanged. Therefore, because of local support, a change in the position of a control point only affects the local portion of the NURBS curve, and this allows great flexibility when trying to approximate grain boundaries accurately. Also, by the local support property,

any modifications to the weights  $w_i$ , too, will only affect the section of the NURBS curve on the  $[u_i, u_{i+p+1})$  interval.

The invariance property of NURBS under affine transformations is useful when updating the grains described using NURBS within the time integration scheme. Exploiting this property, a grain's position is updated by simply translating and/or rotating the control points relative to the grain's centroid.

The strong convex hull property ensures that, for a closed NURBS curve, the entire grain is located within the convex hull defined by the corresponding control points. Using the control points to define a convex hull bounding each grain, the granular entities described using NURBS can be easily incorporated into existing DEM global collision detection algorithms. We note that the control polygon defined by the control points could be non-convex. Also, the convex hull property fails for negative weights in which a portion of the affected curve segment will be outside of the convex hull defined by the corresponding control points. However, negative weights are not typically used when describing grain shapes, and therefore convex hull failure is typically not a concern.

NURBS provides a simple procedure for evaluating local curvatures. It is well known that contact stresses (e.g., Hertzian contact) depend on the radii of curvature of two contacting bodies. Evaluation of curvature for simple shapes such as circles and ellipses is straightforward but becomes complicated for arbitrary-shaped grains. In addition to providing the tangent and normal boundary vectors needed for contact force calculations, NURBS also provide local curvature evaluations that can be used directly in calculating local contact forces. After obtaining the first and second local derivatives  $\mathbf{C}^{(1)}$  and  $\mathbf{C}^{(2)}$ , respectively, the curvature vector can be evaluated such that

$$\boldsymbol{\kappa} = \frac{\left(\mathbf{C}^{(1)} \cdot \mathbf{C}^{(1)}\right) \mathbf{C}^{(2)} - \left(\mathbf{C}^{(1)} \cdot \mathbf{C}^{(2)}\right) \mathbf{C}^{(1)}}{\left(\mathbf{C}^{(1)} \cdot \mathbf{C}^{(1)}\right)^2} \quad (3.10)$$

and consequently, the local radius of curvature is calculated such that  $R = 1/\|\boldsymbol{\kappa}\|$ .

Finally, the use of NURBS provides a foundation for high-fidelity physics at the granular level. Since NURBS have recently been shown to furnish a basis for isogeometric analysis [48], within each particle more complex analysis, such as plasticity, damage, or possibly breakage, can be performed. Evidently, NURBS can offer tremendous flexibility in repre-



senting and optimizing grain morphology, as well as provide important geometric properties that would enable higher-fidelity discrete calculations.

**Remark 3.1.5** *Isogeometric analysis is a computational mechanics technology that uses basis functions emanating from computer aided geometric design (CAGD), such as B-splines, NURBS, and T-splines. It has been shown that isogeometric analysis provides more precise and efficient geometric representations [48].*

**Remark 3.1.6** *The last two of the above features of NURBS have not been considered in this thesis. These can potentially be explored in the future.*

## 3.2 Contact Problem and Implementation

Our earlier work described in [49; 50] has focused on particles geometries that are angular but strictly convex, and the contact algorithms were generalizations of the intersection-based approach used for disks and spheres. While the work has led to improvements in particle morphology representation beyond disks and spheres, it was still limited in two ways. First, the increase in rolling resistance of angular but convex geometries relative to disks is limited. For instance, rolling resistance provided by distributed contact reaction over flat boundaries cannot be represented using strictly convex shapes. Moreover, interlocking behavior between non-convex particles, which contributes significantly to mobilized strength and stability [90; 91], is not accounted for. Second, the generation of strictly convex NURBS shapes is very difficult and restrictive from a modeling perspective. This is even more so when dealing with image data of real particle shapes and obtaining strictly convex boundaries through a fitting procedure is not possible in most cases.

A contact algorithm capable of dealing with general non-convex NURBS particles, to be described in this chapter, would eliminate the above two limitations. As a result, a more faithful representation on the contact force distributions over particle boundaries is obtained and the image data-to-analysis pipeline is significantly streamlined. Without loss of generality, we will work with 3D NURBS surfaces throughout the remaining of this chapter. We also assume that the underlying parametric domain has been normalized, i.e.,  $0 \leq u \leq 1$  and  $0 \leq v \leq 1$  (a unit square).

### 3.2.1 General definition

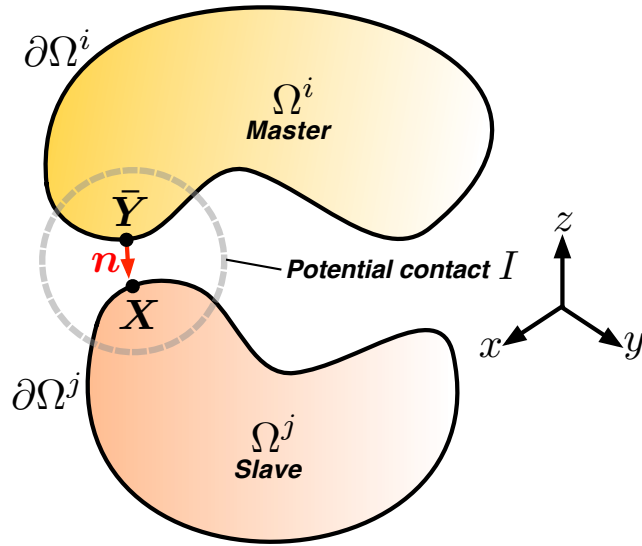


Figure 3.2: Contact problem between two particles  $\Omega^i$  and  $\Omega^j$ . Refer to text for description.

We consider a general two-particle contact problem in three dimensions, with the particles in question to be potentially contacting at some time instant  $t$ . Referring to Figure 3.2, let  $W_i$  be the set of potential contacts associated with particle  $i$ , and denote using  $I \in W_i$  a particular contact point in the set.

Following a master-slave approach to describe the contact problem [92], a contact point on the slave particle  $\Omega^j$  is denoted by  $\mathbf{X}$  while the contact point on the master particle  $\Omega^i$  is defined to be the closest point projection (CPP) of  $\mathbf{X}$  onto the surface of the master particle:

$$\bar{\mathbf{Y}} \equiv \bar{\mathbf{Y}}(\mathbf{X}) = \min_{\mathbf{Y} \in \partial\Omega^i} \|\mathbf{X} - \mathbf{Y}\| \quad (3.11)$$

where  $\|\cdot\|$  is the standard Euclidean norm. As shown in Figure 3.2, the contact plane at a potential contact point  $I$  is described on the master surface  $\partial\Omega^i$  by the outward unit normal  $\mathbf{n}$  at point  $\bar{\mathbf{Y}}$ . The gap or penetration at time  $t$  is then defined as

$$g(\mathbf{X}) = [\mathbf{X} - \bar{\mathbf{Y}}(\mathbf{X})]^T \mathbf{n} \quad (3.12)$$

By this definition, contact penetration occurs if  $g(\mathbf{X}) < 0$ . This convention is similar to

that used in the definition of contact problems in the finite element method (FEM) [92]. In the context of classic DEM [24] with a linear contact law, once the gap is determined, the normal contact force on the master particle is then calculated as (refer to (2.1)):

$$\mathbf{f} = \begin{cases} k_N g(\mathbf{X}) \mathbf{n}, & \text{if } g(\mathbf{X}) < 0 \\ \mathbf{0}, & \text{otherwise} \end{cases} \quad (3.13)$$

where  $k_N$  is the normal contact stiffness. An equal and opposite force acts on the slave particle. Essentially, the contact problem boils down to the problem of solving the CPP problem (3.11) and in the remaining sections, we describe how this is done in the context of NURBS.

### 3.2.2 Knot positioning

We generalize the node-to-surface approach typically used in the contact treatment of finite element models [92] to a ‘knot-to-surface’ (KTS) approach to enable the contact treatment of non-convex particles described using NURBS surfaces. More recently, the KTS approach has been employed in isogeometric finite elements [93] and a similar approach is taken here. The contact points  $\mathbf{X}$  associated with the slave particle are represented through knots and these points are to be projected onto the master surface to determine if there is contact penetration. The representation of contact points through knots is necessary for computational tractability, as well as for tracking the incremental slip and contact gain or loss around non-convex surfaces of potentially contacting particles. While similar to nodal discretization in FEM, we emphasize that the key difference here is that the positioning of contact points by knots does not change the particle geometry, i.e., isogeometric; the knots vary continuously in the underlying parametric space. In this work, we have adopted to position the knots a priori as a preprocessing step.

In real applications where a large number of arbitrary-shaped grains are represented by 3D NURBS surfaces, the manual positioning of knots proved to be extremely difficult, if not impossible. As such, an automatic and adaptive knot positioning strategy is required. To this end, we have devised an automatic knot positioning algorithm based on a NURBS recursive subdivision scheme (see Algorithm 2). The NURBS surface is subdivided until the following termination criteria (see Figure 3.3) are met:

1. Real space arc distance corresponding to each parametric direction of less than  $\epsilon_d$
2. Acute angle between normal vectors at adjacent knot positions of less than  $\epsilon_\theta$

and a knot or node is positioned at the center of the subdivided surface at the terminated level.

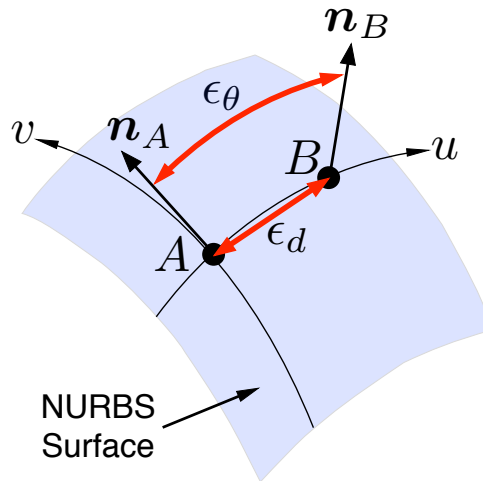


Figure 3.3: Measures used for terminating the NURBS subdivision in the knot or node generation procedure. The two normal vectors emanating from nodes  $A$  and  $B$  are denoted by  $\mathbf{n}_A$  and  $\mathbf{n}_B$ , respectively. NURBS parametric directions are  $u$  and  $v$ .

**Input:** NURBS surface  $S = \mathbf{Y}(u, v)$ , real arc distance tolerance  $\epsilon_d$ , angle tolerance  $\epsilon_\theta$

**Output:** List of knot positions in real space

**procedure** AKP( $S$ )

Calculate the real-space points corresponding to the corners in parametric space:

$$\mathbf{x}_1 = \mathbf{x}(u_{\min}, v_{\min}), \mathbf{x}_2 = \mathbf{x}(u_{\max}, v_{\min}), \mathbf{x}_3 = \mathbf{x}(u_{\max}, v_{\max}), \mathbf{x}_4 = \mathbf{x}(u_{\min}, v_{\max})$$

Calculate real arc distance corresponding to each parametric direction:

$$D_u = \max(\|\mathbf{x}_3 - \mathbf{x}_4\|, \|\mathbf{x}_1 - \mathbf{x}_2\|), D_v = \max(\|\mathbf{x}_1 - \mathbf{x}_4\|, \|\mathbf{x}_2 - \mathbf{x}_3\|)$$

Let  $\Delta u = u_{\max} - u_{\min}$ ,  $\Delta v = v_{\max} - v_{\min}$ ,  $u_{\text{ave}} = (u_{\max} + u_{\min})/2$ ,  
 $v_{\text{ave}} = (v_{\max} + v_{\min})/2$ .

Define acute angle between unit normal vectors  $\theta(\mathbf{n}_1, \mathbf{n}_2) = \cos^{-1}(\mathbf{n}_1 \cdot \mathbf{n}_2)$

**if** ( $D_u > D_v$ )\* **then**

Compute unit normal vectors:  $\mathbf{n}_{u1} = \mathbf{n}(u_{\min} + \Delta u/3, v_{\text{ave}})$ ,

$\mathbf{n}_{u2} = \mathbf{n}(u_{\min} + 2\Delta u/3, v_{\text{ave}})$  and  $\theta_u = \theta(\mathbf{n}_{u1}, \mathbf{n}_{u2})$ .

**if** ( $D_u > \epsilon_d$ ) **and** ( $\theta_u > \epsilon_\theta$ ) **then**

    | Split surface into 2 child surfaces  $S_1, S_2$  at  $u_{\text{ave}}$

**else**

    | Surface is a LEAF

**end if**

**else** ( $D_u \leq D_v$ )\*

Compute unit normal vectors:  $\mathbf{n}_{v1} = \mathbf{n}(u_{\text{ave}}, v_{\min} + \Delta v/3)$ ,

$\mathbf{n}_{v2} = \mathbf{n}(u_{\text{ave}}, v_{\min} + 2\Delta v/3)$  and  $\theta_v = \theta(\mathbf{n}_{v1}, \mathbf{n}_{v2})$ .

**if** ( $D_v > \epsilon_d$ ) **and** ( $\theta_v > \epsilon_\theta$ ) **then**

    | Split surface in into 2 child surfaces  $S_1, S_2$  at  $v_{\text{ave}}$

**else**

    | Surface is a LEAF

**end if**

**end if**

**if** ( Surface is a LEAF ) **then**

    | Store midpoint  $\mathbf{x}(u_{\text{ave}}, v_{\text{ave}})$  as a knot position

**else**

    | Recurse, i.e., apply AKP, on the two child surfaces  $S_1, S_2$

**end if**

**end procedure**

\*For a closed single patch NURBS surface, a seam joins either the edges at (a)  $u = 0, 1$  or (b)  $v = 0, 1$ . At first entry into this procedure, the **if** ( $D_u > D_v$ ) block is executed for case (a) while the **if** ( $D_u \leq D_v$ ) block is executed for case (b).

Algorithm 2: Automatic Knot Positioning (AKP) Algorithm.

### 3.2.3 Distance function

The distance function of a fixed slave point  $\mathbf{X}$  on a slave surface to a master surface  $\mathbf{Y}(u, v)$  is given by

$$d(u, v) = \|\mathbf{X} - \mathbf{Y}(u, v)\| \quad (3.14)$$

or, squaring both sides, we obtain the distance squared function

$$f(u, v) = [\mathbf{X} - \mathbf{Y}(u, v)]^T [\mathbf{X} - \mathbf{Y}(u, v)] \quad (3.15)$$

where  $f(u, v) = [d(u, v)]^2$  and the coordinates of the NURBS surface  $\mathbf{Y}(u, v)$  is given by (3.9).

The CPP problem can then be formulated as (cf. (3.11))

$$\bar{\mathbf{Y}} = \min_{(u,v) \in \Gamma} f(u, v) \quad (3.16)$$

where  $\Gamma$  is the bounded normalized parametric space of the NURBS master surface. In real applications, where surfaces are always well-defined, the underlying NURBS basis functions are products or quotients (with denominators that are bounded away from zero) of univariate B-Splines basis functions, which in turn are polynomials. This implies the distance squared function  $f(u, v)$  is Lipschitz continuous. This means that there exists a finite bound on the rate of change of the squared distance function. This key observation allows one to employ the Lipschitzian *dividing rectangle* (DIRECT) global optimization procedure as a solution to the CPP problem.

### 3.2.4 The DIRECT optimization algorithm

Here, we describe how the DIRECT algorithm can be adapted to the CPP problem (3.16). We describe the following two components of the DIRECT algorithm,

1. Sample and subdivide
2. Identification of potentially optimal parametric rectangles

followed by a simple example to illustrate how the overall DIRECT algorithm works. We emphasize that, in the application of this algorithm, the NURBS surface or underlying

parametric domain is not physically subdivided. The key feature of the DIRECT algorithm is that the subdivisions are performed implicitly through sampling (i.e., function evaluation) and selection of optimal rectangles.

### 3.2.4.1 Sample and subdivide

The basic idea of this step is as follows: the sampling part determines the goodness of the current solution of  $f$  in (3.16), while the subdivision part ensures efficiency as well as convergence of the DIRECT algorithm. After subdivision, the parametric domain will consist of subregions that are either squares or rectangles. We first describe the sample and subdivide step for squares followed by an extension to rectangles.

The basic idea behind the DIRECT algorithm is the sampling of the values of the function  $f$  at the points  $\mathbf{c} \pm \delta \mathbf{e}_i$ ,  $i = 1, 2$ , where  $\mathbf{c}$  is the center of the parametric square,  $\delta$  is one-third side length of the parametric square, and  $\mathbf{e}_i$  is the unit vector in either the  $u$  ( $i = 1$ ) or  $v$  ( $i = 2$ ) direction. Since the underlying parametric domain of the NURBS surface is 2D, the sampling points would be located above, below, to the left, and to the right of the center point (see Figure 3.4(a) or (b)).

The square domain is subdivided such that each subregion (rectangle or square) would contain a sample point at its center. The following strategy for subdividing the square is adopted in [94]. Let

$$w_i = \min \{f(\mathbf{c} - \delta \mathbf{e}_i), f(\mathbf{c} + \delta \mathbf{e}_i)\}, \quad i \in 1, 2 \quad (3.17)$$

be the best of the function values sampled along the  $u$  and  $v$  directions. First, split the square into thirds along the dimension with the smallest  $w$  value. Then, split the rectangle that contains  $\mathbf{c}$  into thirds along the remaining direction. This strategy ensures that the largest subrectangle contains the sample point with the best function value, i.e., lowest  $f$  value. The reason for this strategy is to bias the search near points with good function values, since larger rectangles are preferred for sampling (as a result of convex hull; see below). For rectangular domains, the subdivision is performed only along the long dimension. This ensures that the rectangles shrink in both parametric directions, ensuring convergence [94]. Examples illustrating this subdivision strategy are shown in Figure 3.4. Algorithm 3 formally describes the above steps and covers both square and rectangular domains.

**Input:** A parametric subregion (rectangle or square)

**Output:** A subdivided subregion

- 1: Identify the set  $I \subseteq \{1, 2\}$  with maximum parametric side length in parametric space, where 1 and 2 are in the  $u$  and  $v$  directions, respectively. Let  $\delta$  equal to one-third of this maximum length (if square, pick both sides, otherwise pick longer dimension - see explanation in the text).
- 2: Sample the function at the points  $\mathbf{c} \pm \delta \mathbf{e}_i$  for all  $i \in I$ , where  $\mathbf{c}$  is the center of the parametric rectangle and  $\mathbf{e}_i$  is the  $i$ -th unit vector.
- 3: Divide the rectangle containing  $\mathbf{c}$  into thirds along the dimensions in  $I$ , starting with the dimension lowest value of

$$w_i = \min \{f(\mathbf{c} - \delta \mathbf{e}_i), f(\mathbf{c} + \delta \mathbf{e}_i)\}$$

and continue to the next dimension.

Algorithm 3: Sample and Subdivide Algorithm



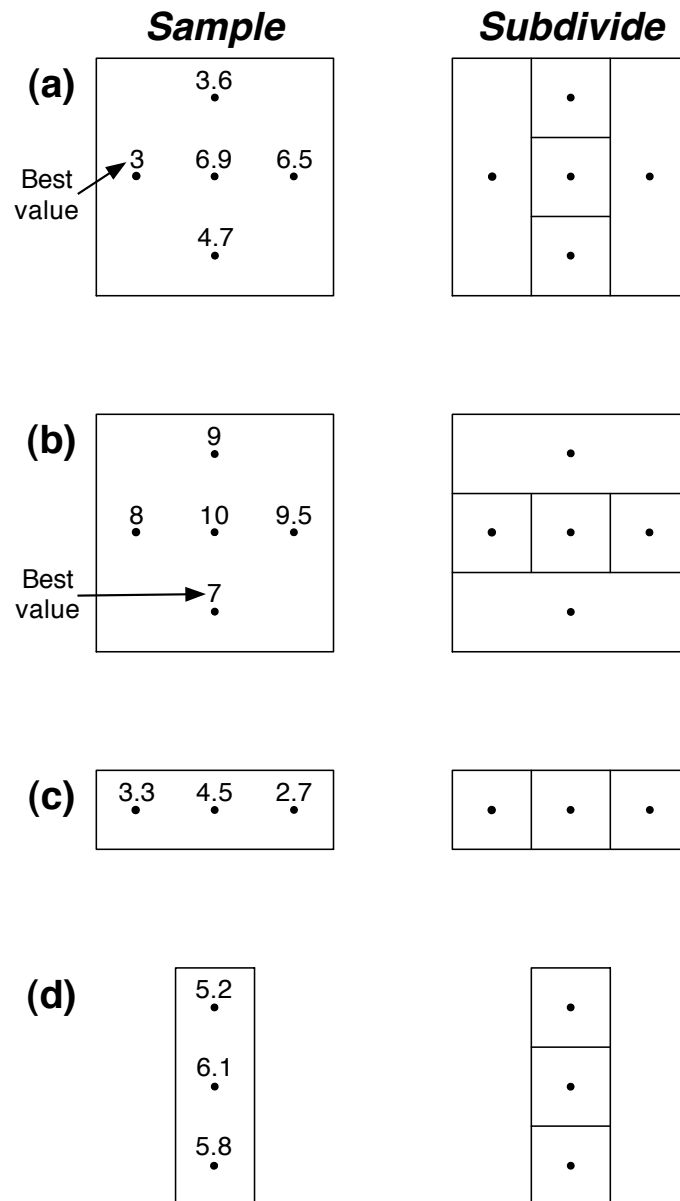


Figure 3.4: Example cases of sample and subdivide. For cases (a) and (b), the domain is square, and the subdivision is such that the largest subrectangles contain the sample points with the best function values, i.e., lower  $f$  values. For cases (c) and (d), the domain is rectangular, and the subdivision is performed only along the long dimension.

### 3.2.4.2 Identification of potentially optimal rectangles

Assume that we have partitioned the unit square parametric domain underlying the NURBS surface into a total of  $m$  rectangles (or squares if the sides are equal). To select optimal rectangles for subdivision, we first compute the following for each rectangle  $j$ :

- Distance from its center to its vertex  $d_j$
- Function value evaluated at the center  $f_j = f(\mathbf{c}_j) = f(u_j, v_j)$

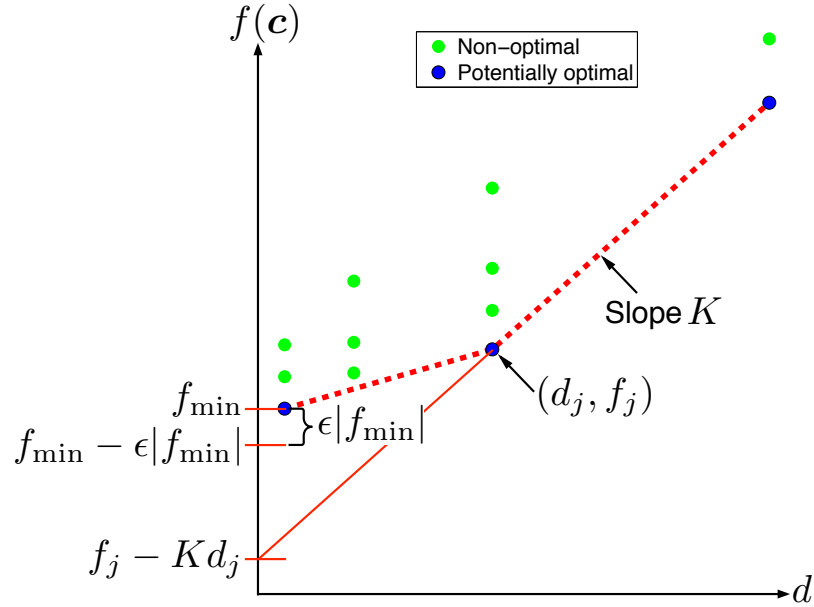


Figure 3.5: A schematic of the graph of  $f(\mathbf{c})$  versus  $d$  for all rectangles in the parametric domain. Refer to the text for the meaning of the labeled quantities.

Then, we plot the points  $(d_j, f_j)$  on a graph with  $f_j$  on the abscissa for all  $j = 1, \dots, m$ , as shown schematically in Figure 3.5. Each point on the graph represents a rectangle in the parametric domain. The set of potentially optimal rectangle is defined as follows.

**Definition 1** Let  $\epsilon > 0$  be a positive constant and  $f_{\min}$  be the best current solution, i.e., the lowest value of  $f$  over all  $m$  rectangles. A rectangle  $j$  is said to be potentially optimal if there exists some  $K > 0$  such that

$$f_j - Kd_j \leq f_i - Kd_i, \quad \forall i = 1, \dots, m \quad (3.18)$$

$$f_j - Kd_j \leq f_{\min} - \epsilon|f_{\min}| \quad (3.19)$$

We note that  $K$  is simply a rate-of-change constant but we can loosely interpret it as a Lipschitz constant. From Figure 3.5,  $f_j - Kd_j$  can be seen as an abscissa intercept, which provides the lower bound for  $f_j$ . The lower bound contains two terms  $f_j$  and  $-Kd_j$ . The first term is lower when the function values are lower. Thus, this term favors locations where previous function values are lower, i.e., emphasis on local search. The second term is lower the larger  $d_j$  becomes. Therefore, this term puts the search emphasis on larger rectangles, i.e., emphasis on global search. As such,  $K$  can also be interpreted as a relative weight on global versus local search. Instead of relying on a single constant  $K$ , which is usually high (too much emphasis on global search) and resulting in slow convergence, the DIRECT algorithm considers all possible weights, and at the same time determines and reduces the weights as the search proceeds. Moreover, the algorithm does not require the a priori specification of the weights, which are usually very hard to estimate or are completely unknown. To see how these are achieved, we observe that geometrically the first condition (3.18) means that the optimal rectangles can be found as the lower right of the convex hull of the set of points in the graph of  $f$  (see dashed red line in Figure 3.5). This means that there is no need to determine  $K$ . The second condition (3.19) prevents the algorithm from becoming too local, at which point too many iterations are performed for marginal improvements. This means that some of the smaller rectangles near the bottom right of the aforementioned convex hull may not be selected. A range of  $10^{-3}$  to  $10^{-7}$  has been suggested but DIRECT is rather insensitive to the choice of  $\epsilon$  [94], due to the convex hull procedure to select potentially optimal rectangles. The convex hull of points can be performed efficiently using the Graham's scan algorithm [95]. If the rectangles are sorted by function value within groups of rectangles with the same center-vertex distance, the resulting computational complexity is  $O(m')$ , where  $m' < m$  is the number of distinct center-vertex distances [94]. For further details on data structures, implementation strategies, and theoretical analysis of the DIRECT algorithm, we refer the reader to [94; 96; 97].

To prevent proliferation of function evaluations as the global minimum is approached, we terminate the DIRECT global search when the relative change in the parameter values is less than some tolerance (e.g.,  $\Delta u/u, \Delta v/v < 0.1$ ) and switch to a local minimization step to finalize the contact point on the master surface. We use the parametric values at termination of the DIRECT global search as an initial guess and a small neighborhood around this initial guess as the search domain. The local minimization problem can be

solved using either gradient-based or derivative-free constrained optimization algorithms [98]. Here, we choose the derivative-free procedure since it is simpler and does not require the evaluation of the Hessian of the function  $f$ .

### 3.2.5 Implementation of contact algorithm

The implementation of the CPP operation can be simply achieved by programming a function handle that returns the squared distance value  $f$  between a given slave contact point  $\mathbf{X}$  and a point  $\mathbf{Y}(u, v)$  on the master surface, and using this function handle in the DIRECT algorithm. The CPP algorithm proceeds as described in Algorithm 4. The one-to-one mapping of the DIRECT algorithm to the CPP problem is particularly noteworthy; except for a few quantities that are relevant to NURBS and the CPP problem, the steps proceed identically with those laid out in [94]. An illustration of the DIRECT algorithm for a few iterations is shown in Figure 3.6. The proposed contact algorithm is then implemented by applying the CPP algorithm on candidate contact points  $\mathbf{X}$  of the slave surface to determine their closest projected points  $\bar{\mathbf{Y}}(\mathbf{X})$ . The penetration is calculated using (3.12), from which the corresponding normal contact force vector on the master particle is then determined by (3.13).

The identification of candidate slave contact points for the CPP operation can be performed through a number of standard collision detection algorithms (e.g., [42]). For example, only those points that are inside the bounding box of the master surface will be considered.

**Input:** Slave point  $\mathbf{X}$  and master surface  $\mathbf{Y}(u, v)$

**Output:** Closest projected point  $\bar{\mathbf{Y}}(\mathbf{X})$

- 1: Let  $\mathbf{c}_1 = (u_1, v_1)$  be the center point of normalized parameter space (unit square) and evaluate  $f(\mathbf{c}_1)$ . Set current best value  $f_{min} = f(\mathbf{c}_1)$ , number of sample points  $m = 1$ , and iteration counter  $k = 0$ .
- 2: Identify the set  $S$  of potentially optimal parametric rectangles.
- 3: Select any rectangle  $j \in S$ .
- 4: Sample and subdivide (see Algorithm 2). Update  $f_{min}$  and  $m = m + \Delta m$  where  $\Delta m$  is the number of new points sampled.
- 5: Remove rectangle  $j$  from set  $S$ . If  $S$  is not empty, go to Step 3.
- 6: Increment iteration counter  $k = k + 1$ . If relative in parametric direction is less than specified tolerance, go to Step 7. Otherwise, go to Step 2.
- 7: Start constrained optimization procedure using current best  $(u, v)$  and corresponding parametric rectangle to finalize the closest projected point on the master surface  $\bar{\mathbf{Y}}(\mathbf{X})$ . Exit.

Algorithm 4: DIRECT Closest Point Projection Algorithm

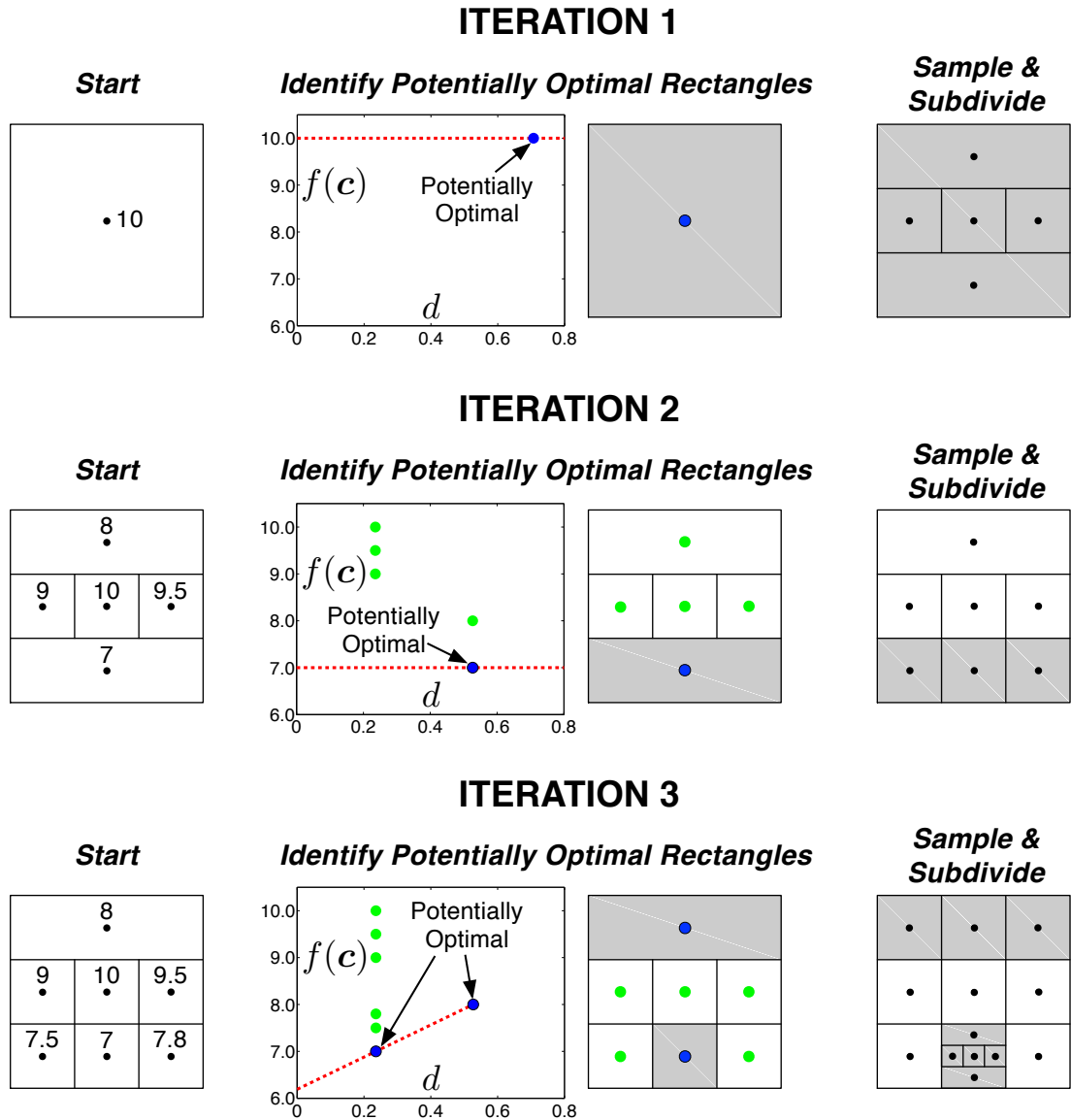


Figure 3.6: Illustration of DIRECT algorithm. For simplicity, we have set  $\epsilon$  in (3.19) to zero. The lines are only to guide the eye — there is no physical subdivision of the NURBS surface or underlying parametric surface; instead the subdivision is performed implicitly through sampling and selection of optimal rectangles.

### 3.3 Closure

We have presented a new algorithm for determining the signed gap value for non-convex NURBS surfaces. The functionality of the algorithm will be demonstrated through discrete simulations described in the next two chapters.